frontiers | Frontiers in Photobiology

TYPE Original Research
PUBLISHED 05 August 2024
DOI 10.3389/fphbi.2024.1387119

OPEN ACCESS

EDITED BY
Jonathan Cohen,
University of Delaware, United States

REVIEWED BY
Stefano Santabarbara,
National Research Council (CNR), Italy
Kazuhiro Yoshida,
Saga University, Japan

*CORRESPONDENCE
Sébastien Guérin,
sebastien.guerin@takuvik.ulaval.ca

†PRESENT ADDRESS
Johann Lavaud, LEMAR-Laboratory of Environmental Marine Sciences, UMR6539 CNRS, University Brest, Ifremer, IRD, Institut Universitaire Européen de la Mer, Technopôle Brest-Iroise, rue Dumont d'Urville, Plouzané, France

RECEIVED 24 March 2024
ACCEPTED 17 July 2024
PUBLISHED 05 August 2024

CITATION
Guérin S, Bruyant F, Gosselin M, Babin M and Lavaud J (2024), Photoperiodic dependent regulation of photosynthesis in the polar diatom *Fragilariopsis cylindrus*.
Front. Photobiol. 2:1387119.
doi: 10.3389/fphbi.2024.1387119

Photoperiodic dependent regulation of photosynthesis in the polar diatom *Fragilariopsis cylindrus*

Sébastien Guérin[1]*, Flavienne Bruyant[1], Michel Gosselin[2], Marcel Babin[1] and Johann Lavaud[1†]

[1]IRL3376 Takuvik, CNRS (France)/ULaval (Canada), Pavillon Alexandre-Vachon, Québec, QC, Canada, [2]Institut des sciences de la mer-Université du Québec à Rimouski, Rimouski, QC, Canada, [3]LEMAR-Laboratory of Environmental Marine Sciences, UMR6539 CNRS, University Brest, Ifremer, IRD, Institut Universitaire Européen de la Mer, Technopôle Brest-Iroise, rue Dumont d'Urville, Plouzané, France

Introduction: Polar microalgae are exposed to dramatic seasonal changes in light availability, from continuous summer days to winter nights with rapid changes of the daylength in spring and fall. Under this challenging light climate, large diatoms spring blooms occur at the bottom sea-ice and underneath the icepack, accounting for a significant proportion of the annual marine primary production in the Arctic Ocean. The on-going earlier melt down of the snow and ice covers result in a stronger light penetration and consequent increase in irradiance at the bottom of the sea ice leading to earlier seasonal sea-ice diatom blooms under shorter daylengths. Therefore, elucidating the response of polar diatoms to different photoperiods will help to better understand the consequences of the changing arctic climate on their photosynthetic productivity.

Methods: In this study, we characterized the response of *F. cylindrus*, a model polar diatom, across five different photoperiods with similar light and temperature conditions (30 µmol photons m^{-2} s^{-1} and 0°C respectively).

Results: We report different photoacclimative strategies under shorter and longer daylengths, with the special case of prolonged darkness (mimicking winter polar night). We also observed a repeated daily regulation of the photochemistry and photoprotection parameters when cells were exposed to a light:darkness alternation, despite the constant and optimal light intensity during the light periods.

Discussion: Our results highlight the ability of *F. cylindrus* to grow efficiently under a wide range of daylengths, finely adjusting the balance between photochemistry and photoprotection to make the best use of the available light, supporting sustained production and growth despite low light and temperature.

KEYWORDS

polar diatom, photosynthesis, photoperiod, pigments, biological rhythm, photoprotection

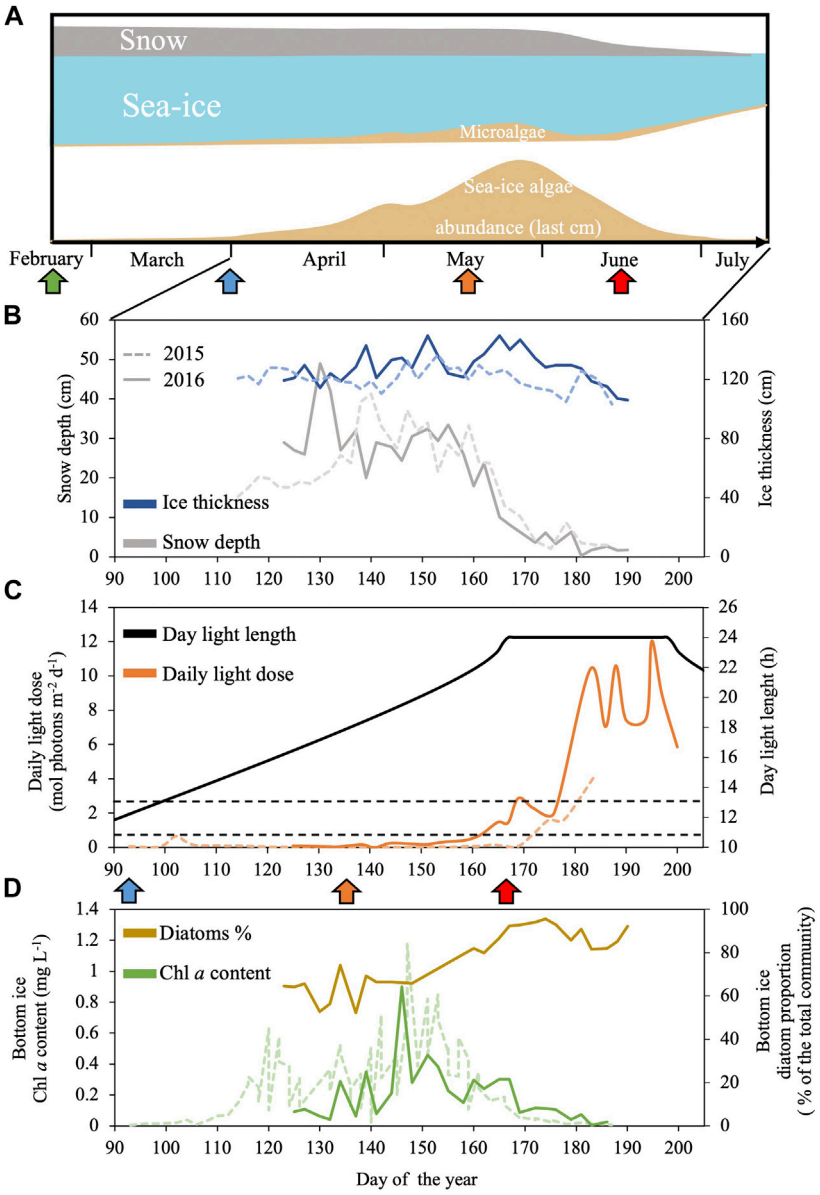

FIGURE 1
Schematic representation of a seasonal dynamics of Arctic sea-ice and associated microalgae from spring to summer in Baffin Bay **(A)** combined with sea-ice environmental conditions and sea-ice algal community abundance and composition assessed during the Green Edge project during spring 2015 (dashed line) and 2016 (continuous line) in the West Baffin Bay (*Qikiqtarjuaq, Nunavut*, 67.48°N 63.79°W): **(B)** Snow depth (grey) and ice thickness (blue); **(C)** daily light dose (orange) and day light length (black); **(D)** Chlorophylla (Chla, green) and diatoms proportion (brown) at the bottom of the sea-ice. Panel **(C)** black dashed lines indicate the minimum and maximum daily light dose used in this study (0.65 and 2.6 mol photons m^{-2} d^{-1}). Panel **(A, C)** the green, blue, orange and red arrows indicate, respectively, the periods where daylength is 6 h, 12 h, 18 h and the first day of 24 h daylength. Data are available at: Green Edge project LEFE-CYBER repository (http://www.obs-vlfr.fr/proof/php/GREENEDGE/greenedge.php); for corresponding Materials and Methods see Massicotte et al. (2020).

1 Introduction

Polar marine microalgae are exposed to dramatic seasonal changes in light availability with rapid changes of the daylength in spring and fall, and between extreme periods of continuous summer days and winter nights which duration depends on latitude (Leu et al., 2015; Hopes et al., 2017). In addition, the light intensity and spectrum perceived by algae at the bottom of the sea-ice varies enormously during the productive season depending on the thickness of the ice- and snow-packs (Figure 1) (Nicolaus et al., 2010; Oziel et al., 2019). Under this challenging light climate, large spring blooms of microalgae, often mostly composed of diatoms, occurs at the bottom sea-ice and underneath the icepack (Figure 1), accounting for a significant proportion of the annual marine primary production in the Arctic Ocean (Leu et al., 2015; Mayot et al., 2018; Ardyna and Arrigo, 2020). Many works have shown how the light-response of polar diatoms is well adapted to low temperatures climate of high latitudes (Petrou et al., 2016;

Lacour et al., 2017; Young and Schmidt, 2020). They can perform photosynthesis and grow efficiently from very low to high light (Hancke et al., 2018; Lacour et al., 2018; Randelhoff et al., 2020; Kvernvik et al., 2021; Croteau et al., 2022). Polar diatoms can also withstand strong light fluctuations and prolonged periods of darkness (Kropuenske et al., 2009; Kennedy et al., 2019; Morin et al., 2020; Croteau et al., 2021; Hoppe, 2021; Joli et al., 2024).

The ecological success of diatoms is notably based on their ability to efficiently respond to changes in their light climate (Wilhelm et al., 2014; Lepetit et al., 2022), particularly in polar (sympagic forms) and benthic (epipelic and epipsammic forms) environments (Petrou et al., 2016; Lacour et al., 2017; Young and Schmidt, 2020). Light-responses are typically of two types: rapid and reversible, and/or more prolonged (several hours and days) (MacIntyre et al., 2000). For prolonged light-responses, diatoms are able to modify the architecture of their photosynthetic apparatus in order to adapt their capacities of absorption and use of light energy (Büchel et al., 2022). To do so, they can for example, modify the pigment composition of their light-harvesting complexes (LHCs) (see Arrigo et al., 2010; Lacour et al., 2018; Croteau et al., 2022 for examples in polar diatoms). For rapid and reversible light-responses (typically less than an hour), diatoms mainly use non-photochemical quenching processes (NPQ), which is also directly depending on above-described long-term modifications, especially the spatial arrangement of LHCs and their pigment composition (Lepetit et al., 2022). The NPQ process is located in the LHCs of photosystems II (PSII), and it dissipates the light energy absorbed in excess (Lavaud and Goss, 2014; Goss and Lepetit, 2015; Lepetit et al., 2022). NPQ is essentially controlled by i) the light-driven xanthophyll cycle pigments, an enzymatic interconversion between diadinoxanthin (Ddx) and diatoxanthin (Dtx) (Lavaud and Goss, 2014; Lacour et al., 2020), ii) the presence and light-dose regulated synthesis of different isoforms of LHC*x* proteins (Taddei et al., 2016; Lepetit et al., 2017; Buck et al., 2019). Excess light dissipation via NPQ is essential to alleviate excitation pressure on PSII, which, if not counterbalanced, results in PSII photodamages and photoinactivation (Campbell and Serôdio, 2020). In polar strains, NPQ is even more crucial because i) low temperatures slow down the enzymatic rate of PSII repair (Petrou et al., 2010; Ni et al., 2017), ii) the PSII repair process mostly takes place during the daily darkness periods in diatoms (Li et al., 2016), hence the spring/summer increase in daylength can generate situations where photodamage can exceed PSII repair, even under moderate irradiance (Campbell and Serôdio, 2020).

The microalgal bottom sea-ice spring bloom can take place under a broad range of photoperiods (from 14 h to 24 h daylength, Figure 1) (Massicotte et al., 2020). As the snow and ice covers melt down earlier, due to the arctic climate warming (Rantanen et al., 2022), there is a general increase in light penetration to the sea-ice bottom in the Arctic Ocean. The increase in light availability can supports an earlier sea-ice bloom under photoperiods with shorter daylengths (Ardyna and Arrigo, 2020). The response of diatoms to variations in light intensity was extensively studied (Lepetit et al., 2022), but so far, few studies have addressed the impact of the diurnal cycle only (i.e., isolated from changes in irradiance) on their photobiology (Falciatore et al., 2022). The limited number of works on the response of diatoms to daylength is even more concerning in polar strains. Therefore, elucidating the response of polar diatoms to different photoperiods is arguably one of the keys to better understand their productivity and ecological success as well as the ecosystem reaction to the changing Arctic Ocean climate. *Fragilariopsis cylindrus* is the model polar diatom which genome has been sequenced (Mock, 2017) and metabolic network modeled (Lavoie et al., 2020). It is abundant at both poles, and it is found in sea-ice and the water column, mostly underneath the sea-ice pack. *F. cylindrus* shows a large number of LHCx isoforms (11, Mock et al., 2017) as well as an effective NPQ and xanthophyll cycle at circa 0°C temperatures (Arrigo et al., 2010; Croteau et al., 2021). In a series of recent works, we have documented *F. cylindrus* growth to a range of irradiances (Croteau et al., 2022), its response to short-term excess light (Croteau et al., 2021), and to prolonged darkness (several weeks) and return to light (Morin et al., 2020; Joli et al., 2024). Complementary to these works, it is the objective of this study to characterize the features of *F. cylindrus* response across five seasonal arctic photoperiods.

2 Materials and methods

2.1 Culturing conditions

Culturing and all experiments were performed in a climate control "cold" laboratory where temperature was set at 0°C and humidity (<50%, dew point −10°C) was permanently controlled. Culturing and experiments were performed in axenic conditions inside the temperature-controlled laboratory. Axenic *F. cylindrus* (CCMP3323) was grown in natural seawater (sampled in Baffin Bay, Canadian Arctic, 67.48 N; 63.79 W) enriched with f/2 (Guillard, 1975). The sea water was prefiltered through a polypropylene 1 µm filter (Polypropylene felt filter bag 18–1/2L, 1 µm, Cole Parmer, Canada) and sterilized with a PolyCap 0.2 µm (Whatman™, United Kingdom). Cultures were pre-acclimated to each experimental light conditions for at least 3 weeks before the start of the experiment; they were gently stirred with a magnetic stirrer and aerated with air bubbling filtered through an activated carbon filter and a 0.2 µm HEPA filter (Carbon CAP, HEPA-Vent, Whatman™, United Kingdom). Cells were grown in triplicate in 3 L jacketed cylinder reactors at the temperature of 0°C. The temperature was controlled by the circulation of thermostated ethylene glycol through the jacket. Light was supplied uniformly by a custom illumination system with an array of LEDs (LXML-PR01, 445 nm; LXML-PB01, 470 nm; LXML-PM01, 505 nm; LXML-PM01, 530 nm; LXM2-PD01, 630 nm; LXM3-PD01, 660 nm; LXML-PD01, 4100 K; LXML-PL01, amber; LUXEON REBEL, LUMILEDS, Germany) that allowed the modulation of light intensity, the photoperiod and the recreation of a "white" light similar to under sea-ice solar spectrum (Supplementary Figure S1). PAR (Photosynthetically Available Radiations) light intensity was measured continuously in the centre of each reactor using a 4π PAR sensor (QSL 2101, Biospherical Instruments Inc., CA, United States) and PAR intensity was automatically adjusted according to the continuous reading of the PAR sensor to maintain PAR intensity inside the reactor vessel to the targeted value. To better highlight the responses to photoperiod changes, the optimal light intensity for the growth of *F. cylindrus* was used, i.e. 30 µmol photons m^{-2} s^{-1} of PAR (Morin et al., 2020; Croteau et al., 2022). Importantly, cultures were maintained optically thin, in order to control the light field inside the reactors, by a daily dilution semi-continuous growing to maintain a cell concertation of 10^6 cells mL^{-1}.

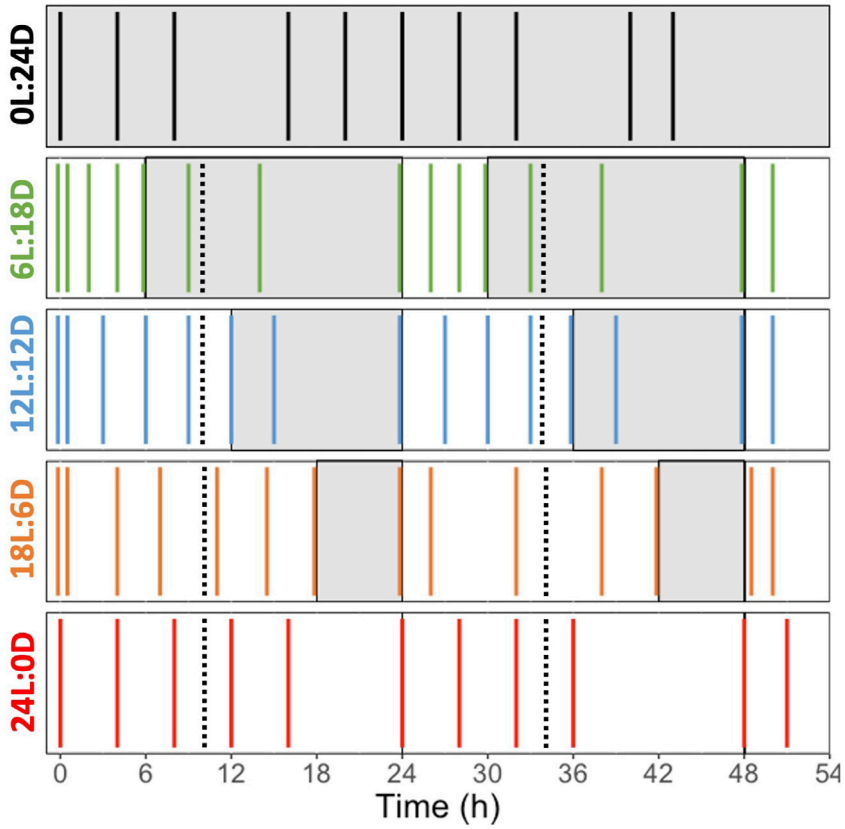

FIGURE 2
Sampling schedule during the experiments performed on *Fragilariopsis cylindrus* cells acclimated to five different photoperiods: 0 h Light: 24 h Darkness (0L:24D, dark), 6L:18D (green); 12L:12D (blue); 18L:6D (orange); 24L:0D (red). The white and grey sections correspond to the light and darkness phases, respectively. The black dashed lines represent the dilution point and the colored solid line represent the sampling point. The photoperiod color code is the one used all along the manuscript.

2.2 Experimental conditions and sampling plan

The cells were acclimated to five photoperiods: 0 h Light: 24 h Dark (0L:24D), 6L:18D, 12L:12D, 18L:6D and 24L:0D (Figure 2). Each experiment lasted 52 h, and the time laps between samplings was at minimum 2 h and at maximum 6 h to perform cell counts, samplings for pigment analyses and measurements of photosynthetic performance (i.e., Rapid Light Curves, see below). The time laps between sampling were adjusted depending on the daylength and the moment of the day, for a tighter coverage during the light compared to the dark period. At the last sampling point, samples were taken for elemental composition analysis and photosynthetic carbon fixation estimation (Production Light Curves, see below). All measured parameters, their definition and unities are found in Table 1. All samplings and measurements were performed in the temperature-controlled laboratory under a green light of low intensity to prevent light alteration of cell photosynthetic activity and pigments. Cultures acclimated at 0:24 were not diluted, the cultures acclimated 6L:18D, 12L:12D, 18L:6D were diluted during the first hour of the dark period of the photoperiods and the cultures acclimated at 24:0 were diluted at the 10th hour of the 24 h cycle.

2.3 Cell concentration and growth rate

Cell concentration was measured using a particle sizing and counting analyser (Multisizer 4 Coulter Counter, Beckman Coulter, United States). We considered counts between 2 and 15 µm cell size. A dilution of the culture sample was performed before analysis to remain within the cell concentration measurement range of the analyser. Dilution was carried out with the electrolyte of the analyzer, i.e., salted Milli-Q™ water (35 g L^{-1}. NaCl). The growth rate (µ, in day^{-1}) was calculated between two dilutions according to Andersen (2005), and the hourly growth rate (μ^H, in h^{-1}) between two sampling points.

2.4 Particulate organic carbon and nitrogen determination

The total particulate carbon (TPC), total particulate nitrogen (TPN), and the dry algal biomass were determined by filtering culture samples on pre-burned (450°C for 4 h) 25 mm GF/F glass-fibre filters (Whatman™, United Kingdom). The CHN analyses were performed with a PerkinElmer 2,400 Series II CHNS/O elemental analyzer (PerkinElmer, Waltham, United States). Acetanilide (99.999%, Perkin Elmer) was used as a standard.

TABLE 1 Synthesis of all parameters measured in this study.

	Measurement	Parameter (short name, unit.)
Measured for each sampling point	Rapid Light Curve (rETR vs. E-light intensity)	Dark-acclimated photochemical efficiency (F_V/F_M, rel. unit.)
		Maximum relative electron transport rate ($rETR_{max}$, µmol electrons $m^{-2}s^{-1}$)
		Light usage efficiency (α, µmol electrons $m^{-2}s^{-1}$ per µmol photons m^{-2} s^{-1})
		Light saturation coefficient (E_k, µmol photons m^{-2} s^{-1})
		Light intensity for reaching $rETR_{max}$ (E_{opt}, µmol photons m^{-2} s^{-1})
	Rapid Light Curve (NPQ vs. E)	Maximal NPQ induced for the highest intensity of the Rapid Light Curve (NPQ_{max}, rel. unit.)
		Light intensity for reaching 50% of NPQ_{max} ($E50_{NPQ}$, µmol photons $m^{-2}s^{-1}$)
	PS II excitation allocation	Quantum yield of photochemical energy conversion in photosystem II (PSII, ϕ_{PSII}, rel. unit.)
		Quantum yield of regulated non-photochemical energy loss in PSII (ϕ_{NPQ}, rel. unit.)
		Quantum yield of non-regulated non-photochemical energy loss in PSII (ϕ_{NO}, rel. unit.)
	Pigment content	Intracellular Chlorophyll *a* content (Cellular Chl *a*, pg $cell^{-1}$)
		Chlorophyll *c* (Chl *c*, mol 100 mol Chl a^{-1})
		Fucoxanthin (Fx, mol 100 mol Chl a^{-1})
		β -Carotene (β-Car, mol 100 mol Chl a^{-1})
		Diadinoxanthin (Ddx, mol 100 mol Chl a^{-1})
		Diatoxanthin (Dtx, mol 100 mol Chl a^{-1})
		De-epoxidation state (DES, %)
		Sum of photosynthetic pigments (P_{PH}, pg $cell^{-1}$, Chl *a*+Chl *c* + Fx+β-Car)
	Cell count	Cells concentration (cells, mL^{-1})
		Growth rate (µ, d^{-1})
		Hourly growth rate (μ^H, h^{-1})
Measured after 52 h of experiment	Elemental composition	Intracellular Carbon content (Cellular C, pg $cell^{-1}$)
		Intracellular Nitrogen content (Cellular N, pg $cell^{-1}$)
		Carbon-Nitrogen ratio (C/N, g g^{-1})
		Chlorophyll *a* -Carbon ratio (Chl *a*/C, mg g^{-1})
		Dry weight (dw, mg L^{-1})
	Photosynthesis vs .light intensity-(P-E curves)	Maximal Carbon fixation (P_{max}, mg C mg Chl a^{-1} h^{-1})
		Net primary production (NPP, mg C mg Chl a^{-1} d^{-1})
		Gross primary production (GPP, mg C mg Chl a^{-1} d^{-1})
		Light usage efficiency (P-α, mg C mg Chl a^{-1} h^{-1} per µmol photons m^{-2} s^{-1})
		Light saturation coefficient (P-E_k, µmol photons m^{-2} s^{-1})
		Light intensity for reaching P_{max} (P-E_{opt}, µmol photons m^{-2} s^{-1})

2.5 Pigment extraction and quantification

Pigments were quantified by High Performance Liquid Chromatography (HPLC, Agilent Technologies 1,200 Series, Agilent, United States). Culture samples were filtered onto 25 mm GF/F glass fiber filters (Whatman™, United Kingdom) in the cold laboratory, immediately frozen in liquid nitrogen and stored at −80°C until further analysis. Before extraction, 50 µL of

internal reference apo-carotene (trans-b-Apo-80-carotenal, 1.98 mg L^{-1}) was added to the 3 mL extraction buffer (100% methanol HPLC grade) for each sample and to the blanks. Filters were ground by sonication (Sonicator Ultrasonic Processor XL 2010) for 12 s on ice and centrifuged for 5 min at 3,700×g. The extracts were filtered through a 0.22 µm polytetrafluoroethylene syringe filter and placed in an automatic sampling vials filled with argon to limit oxidation. A volume of 100 µL was injected into a C8 Symmetry® column (150 × 4.6 mm; 3.5 µm, Waters, France) of the HPLC system. Elution by the solvent gradient was monitored by a P4000 Thermo Separation (TSP) pump as indicated in Zapata et al. (2000). The pigments were detected with a TSP UV 6000 LP absorbance detector (400–700 nm). Pigment quantification was carried out using pigment standards provided by D.H.I. Water & Environment (Horsholm, Denmark) and the internal reference (apo-carotene). The de-epoxidation state of diadinoxanthin in diatoxanthin (DES) was calculated as in Equation 1:

$$DES = \frac{Dtx}{Ddx + Dtx} \times 100 \quad (1)$$

2.6 Photosynthetic performance

A blue light source (λ = 450 ± 20 nm) Pulse Amplitude Modulated (PAM) fluorometer (WATER-ED/B, Heinz Walz GmbH, Germany) was used to measure the photosynthetic performance of cultures on dark acclimated (30 min) samples. Rapid Light Curves (RLCs) were performed with eight 30 s steps of increasing light intensity from 0 to 420 µmol photons m^{-2} s^{-1}. The dark-acclimated photochemical efficiency of photosystem II (PSII, F_V/F_M) was calculated as in Equation 2:

$$F_V/F_M = \frac{F_M - F_0}{F_M} \quad (2)$$

were F_0 and F_M are, respectively, the minimum and maximum levels of dark acclimated chlorophyll fluorescence. The relative electron transport rate (rETR) was calculated as in Equation 3:

$$rETR = E \times \frac{F_M' - F'}{F_{M'}} \quad (3)$$

where E is the light intensity, and F' and F_M' are, respectively, the steady-state and maximum fluorescence levels of light acclimated cells. The determination of rETR for each of the eight intensities of the RLCs allowed to build rETR vs. E curves that were fitted according to Eilers and Peeters (1988) in order to extract photosynthetic parameters (see Barnett et al., 2015): $rETR_{max}$, α, E_k, and E_{opt}; see Supplementary Table S1 for definitions.

The ouput of the RLCs also allowed to calculate the non-photochemical quenching (NPQ) as in Equation 4:

$$NPQ = \frac{(F_M - F_M')}{F_M'} \quad (4)$$

The determination of NPQ for each RLCs step allowed to build a NPQ vs. E curve used to estimate $E50_{NPQ}$ by fitting it with the model of Serodio and Lavaud (2011). Additionally, the maximal NPQ (NPQ_{max}) was the maximal value obtained for the highest RLC step (420 µmol photons m^{-2} s^{-1}).

The partitioning of absorbed excitation energy in PSII was determined by the complementary PSII quantum yields method (Hendrickson et al., 2004; Klughammer and Schreiber, 2008; Xu et al., 2019), and computed as: $\Phi_{PSII} = (\frac{F_M' - F'}{F_M'})$, $\Phi_{NPQ} = \frac{F'}{F_M'} - \frac{F'}{F_M}$ and $\Phi_{NO} = (\frac{F'}{F_M})$; (see Table 1 for definitions).

Under our growth conditions, *F. cylindrus* shows an absorption coefficient of 0.86 (unitless) for the Water-PAM blue light (450 nm) and of 0.39 (unitless) for the growing "white" light spectrum. F' and F_M' were measured during RLC at 16 µmol photons m^{-2} s^{-1} providing 13.8 µmol photons m^{-2} s^{-1} of photosynthetic useable radiation, PUR, equivalent to 34.5 µmol photons m^{-2} s^{-1} of "white" light PAR as used for the photoperiod treatments (i.e., the RLC light intensity the closest to our experimental PAR of 30 µmol photons m^{-2} s^{-1}). Absorption coefficient and PUR were calculated as described by Guérin et al. (2022).

2.7 Production performances

The production vs. light curve (P vs. E, Steeman-Nielsen, 1975) were measured by adding 20 µL of a solution of 74 MBq mL^{-1} of $H^{14}CO_3$ (GE Healthcare, United States) to 40 mL of a culture sample. Then, 28 subsamples of 1 mL were illuminated for 20 min at increasing light intensities from 0 to 442 µmol m^{-2} s^{-1} photons at 0°C. Furthermore, six supplementary sub samples were incubated for 20 min and 24 h, under the culture respective growth light intensity and photoperiods (for 24 h incubation), to quantify the net and gross primary production respectively (NPP and GPP). Immediately after the extinction of the light, 50 µL of buffered formalin was added to each incubation vial to stop the reaction. Samples were acidified with 250 µL of 50% HCl (v./v.) for at least 3 h to allow the venting of inorganic ^{14}C (Poulain et al., 2014) before liquid scintillation counting in a Tri-Carb2910 TF (Perkin Elmer, United States). The P vs. E curves were fitted to the equation of Eilers and Peeters (1988) to compute the parameters P_{max}, P-α, P-E_k and P-E_{opt} (see Table 1 for definitions).

2.8 Statistical analysis

A one-way ANOVA followed by Tukey's HSD *post hoc* test were used to tests differences in the measured parameters means between treatments (Supplementary Table S1). Normality of residuals and homogeneity of variances were tested using Shapiro-Wilk and Bartlett's test respectively. Analysis were performed using R version 4.2.2 (2022-10-10).

3 Results

3.1 Photoacclimation to seasonal photoperiod

The growth rate (µ, Figure 3A) increased with daylength and reached its maximum (0.25 ± 0.04 d^{-1}) for the cells acclimated to 18 h Light: 6 h Dark (18L:6D). P_{max} (Figure 3; Table 1 for the definition of all parameters) decreased with increasing daylength and was close to 0 under 0L:24D. The gross primary production (Figure 3B)

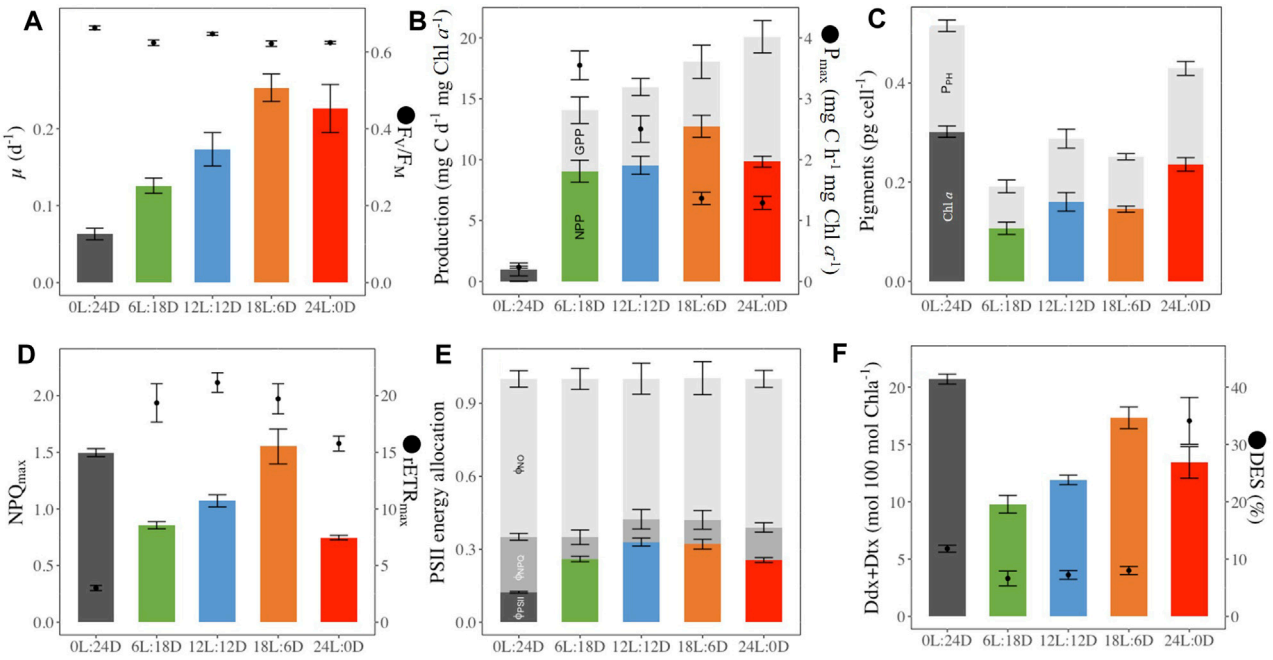

FIGURE 3
Photophysiological parameters in (F) *cylindrus* grown under five different photoperiods 0 h Light: 24 h Darkness (0L:24D), 6L:18D; 12L:12D; 18L:6D; 24L:0D. Daily growth rate (μ, d^{-1}, histograms panel **(A)**, dark-acclimated photochemical efficiency (F_V/F_M, rel. unit, dots panel **(B)**; Gross (GPP, mg C d^{-1} mg Chl*a*$^{-1}$, sum of color and grey histograms panel **(B)** and Net (NPP, mg C d^{-1} mg Chl*a*$^{-1}$, colored histograms panel **(B)** primary production, maximal carbon fixation (P_{max}, mg C h^{-1} mg Chl*a*$^{-1}$, dots panel **(B)**; cellular chlorophyll*a* (Chl*a*, pg $cell^{-1}$, colored histograms panel **(C)** and sum of photosynthetic pigments including Chl*a* (P_{PH}, pg $cell^{-1}$, grey histograms panel **(C)**; maximal non-photochemical quenching (NPQ_{max}, rel. unit colored histograms panel **(D)**, maximum relative electron transport rate ($rETR_{max}$, μmol electrons m^{-2} s^{-1}, dots panel **(D)**; quantum yield of non-regulated non-photochemical energy loss in PSII (ϕ_{NO}, rel. unit, light grey histograms panel **(E)**, quantum yield of regulated non-photochemical energy loss in PSII (ϕ_{NPQ}, rel. unit. grey histograms panel **(E)**, quantum yield of photochemical energy conversion in photosystem II (ϕ_{PSII}, rel. unit. colored histograms panel **(E)**; photoprotective xanthophyll pool per 100 Chlorophyll*a* (Ddx + Dtx, mol 100 mol Chl*a*$^{-1}$, colored histograms panel **(F)**, de-epoxidation stated (DES, %, dots panel **(F)**. Data are the mean values of independent biological triplicates; sampling at the last time point for μ, GPP, NPP, P_{max}, or averaged over the 52 h of monitoring for the other parameters.

increased with the daylength, while the net primary production (Figure 3B) followed the same trend as the growth rate. The intracellular C (Table 2) was maximal for 6L:18D cells (19.2 ± 2.7 pg $cell^{-1}$) and decreased with the increase in daylength until reaching a minimum for 18L:6D (3.10 ± 0.5 pg $cell^{-1}$). The C/N (Table 2) was relatively similar between photoperiods (around 5.1 ± 0.5 g g^{-1}) as well as the Chlorophyll *a* (Chl *a*)/C (20.2 ± 5.0 mg g^{-1}), although the lowest and highest were observed under 6L:18D and 24L:0D, respectively.

Intracellular Chl *a* (Figure 3) increased with daylength, and the highest values were observed at both extreme photoperiods (0L:24D and 24D:0L, Figure 3). The photosynthetic pigments (Chl *c* and β-Carotene, fucoxanthin, Figure 3; Table 2) remained stable relative to Chl *a* among photoperiods, at the exception of fucoxanthin which decreased with daylength. Photoprotective Ddx and Dtx (Table 2) contents nearly doubled from 6 h to 18 h daylength and reached a maximum under 0L:24D (20.7 ± 0.6 mol 100 mol Chl a^{-1}). The de-epoxidation state of Ddx into Dtx (DES, Figure 3) was low and similar (average 7.3% ± 0.7%) under 6L:18D, 12L:12D and 18L:6D and reached a significant maximum under 24L:0D (34.1% ± 4.6%).

F_V/F_M (Figure 3) was the highest under 0L:24D (0.660 ± 0.005) and 12L:12D (0.65 ± 0.01). No significant differences have been found between the three other treatments with a value of 0.62 ± 0.01. Φ_{PSII} (Figure 3) was maximal for 12L:12D and 18L:6D growing cells and divided by a factor of three under 0L:24D. $rETR_{max}$ (Figure 3) was similar for 6L:18D and 12L:12D growing cells (average 21.1 ± 1.0) and the lowest under 0L:24D. NPQ_{max} (Figure 3) was the highest under 0L:24D and 18L:6D (1.5) and halved under 24L:0D. Φ_{NPQ} (Figure 3) was maximal under 0L:24D and halved under the other light conditions (average 0.10 ± 0.03) while Φ_{NO} was similar under all photoperiods (average 0.61 ± 0.04). $E50_{NPQ}$ (Table 2) was the highest under 12L:12D (152 ± 39 μmol photons m^{-2} s^{-1}) and the lowest under 24L:0D and 0L:24D.

3.2 Photoperiodic regulation of photosynthesis

Beyond the above described photoacclimation status based on average ± SD of three independent cultures monitored during 52 h, many of the examined parameters showed daily variations under light:darkness alternation, although the light intensity was kept stable (30 μmol photons m^{-2} s^{-1}) during the light period.

Cultures grown under 6L:18D, 12L:12D and 18L:6D regimes showed a steady increase of the hourly growth rate (μ^H, h^{-1}, Figure 4A) from the beginning of the light period reaching a maximum after 4–6 h, followed by a plateau (12L:12D and 18L:6D treatments), and a decrease to a minimum during darkness

TABLE 2 Photophysiological parameters in *F. cylindrus* cells acclimated to five different photoperiods.

Photoperiod (Light:Dark hours)		0L:24D	6L:18D	12L:12D	18L:6D	24L:0D
Growth, Elemental composition and Production	Cellular C	13.7 ± 1.1	19.2 ± 2.7	10.6 ± 1.2	3.10 ± 0.5	11.2 ± 0.7
	C/N	5.66 ± 0.05	5.00 ± 0.3	4.92 ± 0.06	5.43 ± 0.2	4.63 ± 0.2
	Chl *a*/C	20.6 ± 0.7	15.3 ± 3.3	20.7 ± 2.8	20.1 ± 1.9	24.3 ± 0.1
	P-α	0.11 ± 0.02	0.16 ± 0.02	0.08 ± 0.01	0.08 ± 0.01	0.04 ± 0.02
	P-E_k	2.10 ± 0.1	22.2 ± 0.9	29.4 ± 1.7	35.7 ± 4.2	16.1 ± 0.8
	P-E_{opt}	111 ± 27	180 ± 13	219 ± 4.7	137 ± 7.1	93.3 ± 6.0
Photosynthetic pigments	Chl *c*	19.1 ± 0.8	21 ± 1.2	21.2 ± 1.2	21 ± 2.4	22 ± 1.3
	Fx	57.0 ± 2.0	66.4 ± 6.5	55.5 ± 1.7	48.8 ± 3.2	57.3 ± 2.7
	β-Car	2.30 ± 0.08	3.30 ± 0.75	2.88 ± 0.13	2.75 ± 0.2	2.74 ± 0.08
Photoprotection pigments	Ddx	18.3 ± 0.6	9.41 ± 3.1	11.1 ± 1.4	15.9 ± 2.1	8.8 ± 0.63
	Dtx	2.44 ± 0.13	0.66 ± 0.37	0.87 ± 0.36	1.38 ± 0.48	4.63 ± 0.97
Photosynthetic parameters	α	0.18 ± 0.02	0.33 ± 0.06	0.38 ± 0.04	0.39 ± 0.05	0.30 ± 0.02
	E_k	14.8 ± 1.6	58.1 ± 11	57.4 ± 8.5	56.2 ± 8.6	52.5 ± 1.8
	E_{opt}	63.8 ± 5.6	154 ± 19	156 ± 22	153 ± 18	187 ± 8.5
Non-photochemical quenching	$E50_{NPQ}$	32.7 ± 1.3	91.7 ± 10.0	152 ± 39	117 ± 33	43.6 ± 4.0
	NPQ_{max}/Ddx + Dtx	0.07 ± 0.007	0.09 ± 0.03	0.10 ± 0.03	0.09 ± 0.03	0.055 ± 0.01
	NPQ_{max}/Dtx	0.61 ± 0.06	1.64 ± 1.4	1.53 ± 0.96	1.30 ± 0.69	0.18 ± 0.04
ETR and NPQ derived parameters	$E50_{NPQ}/E_k$	2.20 ± 0.20	1.62 ± 0.35	2.67 ± 0.57	2.21 ± 0.47	0.75 ± 0.13
	E_{opt}/E_k	4.35 ± 0.45	2.58 ± 0.41	2.68 ± 0.36	3.00 ± 0.28	3.57 ± 0.15
	$E50_{NPQ}/E_{opt}$	0.52 ± 0.06	0.58 ± 0.09	0.99 ± 0.36	0.76 ± 0.13	0.27 ± 0.05

Data correspond to the average value for all sampling points for a triplicate of cultures for each photoperiod. For the growth, elemental composition and production data correspond to the last sampling time point. For parameters definition and units see Table 1.

(Figure 4A). In parallel, F_V/F_M (Figure 4B) rapidly increased during the first hours of the light period, reaching a maximum before the middle of the light period. F_V/F_M decrease systematically started before the onset of the darkness period, and continuing until light onset (Figure 2B b, 6L:18D, 12L:12D and 18L:6D). This pattern was modelled onto the length of the light period (i.g. the longer the light period, the later the value reach is maximum) and repeated itself over the next 24 h of monitoring. In contrast, F_V/F_M values were stable under treatments with no light:darkness alternation (Figure 4B, 0L:24D and 24L:0D). Other photosynthetic and photoprotective parameters ($rETR_{max}$, NPQ_{max}, Figures 5A, B), as well as the photoprotective pigments (Ddx + Dtx, DES, Figure 5C; Supplementary Figure S8) showed a similar pattern of daily variations with some modulations, while all of them showed the same stable pattern as F_V/F_M under 0L:24D and 24L:0D (Supplementary Figures S2–S12).

However, different types of patterns were observed during the light period: i) decrease after reaching their daily maximum (i.e., $rETR_{max}$ NPQ_{max} and Ddx + Dtx Figure 5 also E_k, E_{opt}, ϕ_{PSII} Supplementary Figures S2, S3, S5), ii) a steady increase during the light period for reaching a maximum at the light-darkness transition (i.g. $E50_{NPQ}$ and ϕ_{PSII}, Supplementary Figures S5 and S7) at the exception of the 18L:6D which fall in to the first group, iii) decrease during the first hours of illumination before increasing again (ϕ_{NO} Supplementary Figure S6). Also, for some parameters, 6L:18D cells showed a different pattern than 12L:12D and 18L:6D cells: i) E_k 6L:18D (Supplementary Figure S2) showed an inversed pattern compared to 12L:12D and 18L:6D cells, i.e., it decreased at light and increased under darkness; ii) NPQ_{max} 6L:18D (Figure 5B) was stable under darkness when it increase for 12L:12D and 18L:6D cells; iii) Ddx + Dtx 6L:18D (Figure 5C) reached its maximum by the end of the light period instead of the middle for 12L:12D and 18L:6D cells; iv) 6L:18D β-Carotene synthesis (Supplementary Figure S12) showed daily variations when it was steady for 12L:12D and 18L:6D cells.

When plotted as a function of the Zeitgeber Time (ZT), a standardized 24-hour cycle where 0 indicates the beginning of the illumination and 12 the end of the illumination, and as a function of the cumulative light dose (LD) received over the daylight period (Figure 6), some synchronisation appeared either with ZT and/or LD, depending on parameters. Most photosynthetic parameters daily oscillations were synchronized with the light period, reaching their maximum around the sixth hour of ZT (F_V/F_M and $rETR_{max}$, Figures 6A, B) but also earlier at the fourth hour (α and E_{opt}, Supplementary Figures S14A, C). The same holds true for the photochemistry energy usage with maximum at the fourth, 6 and 10thh, for Φ_{PSII}, Φ_{NO} and Φ_{NPQ} respectively

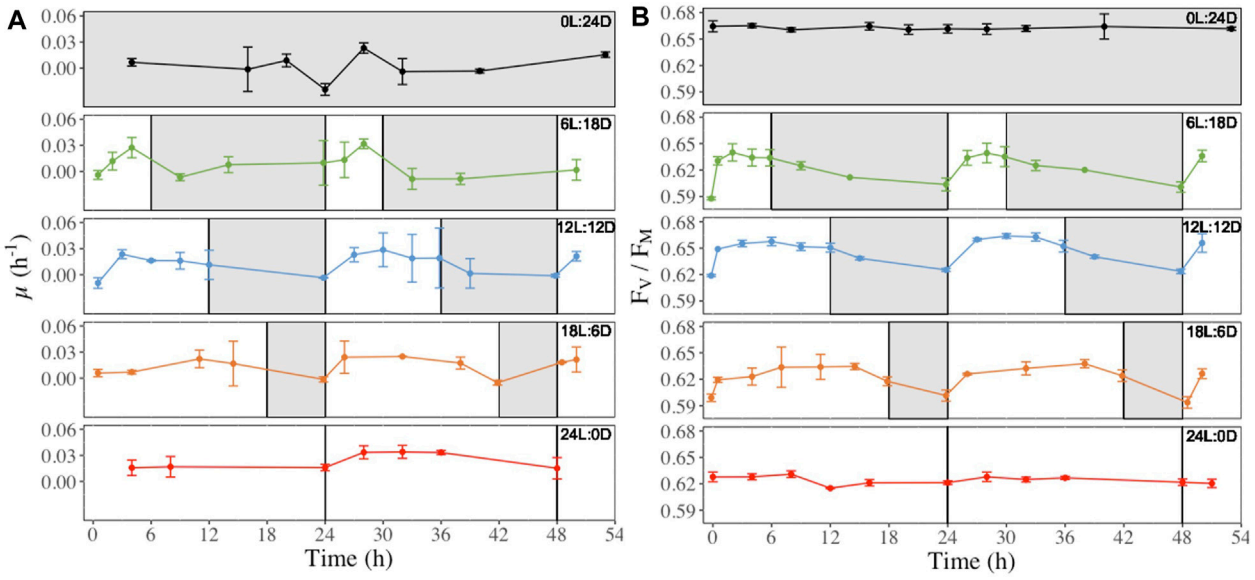

FIGURE 4
Hourly growth rate (μ^H, h^{-1}, panel **(A)** and dark-acclimated photochemical efficiency (F_V/F_M, rel. unit, panel **(B)** recorded at regular time points over 52 h in (F) *cylindrus* grown under five different photoperiods 0 h Light: 24 h Darkness (0L:24D), 6L:18D; 12L:12D; 18L:6D; 24L:0D. The white and grey sections correspond to the light and darkness periods, respectively.

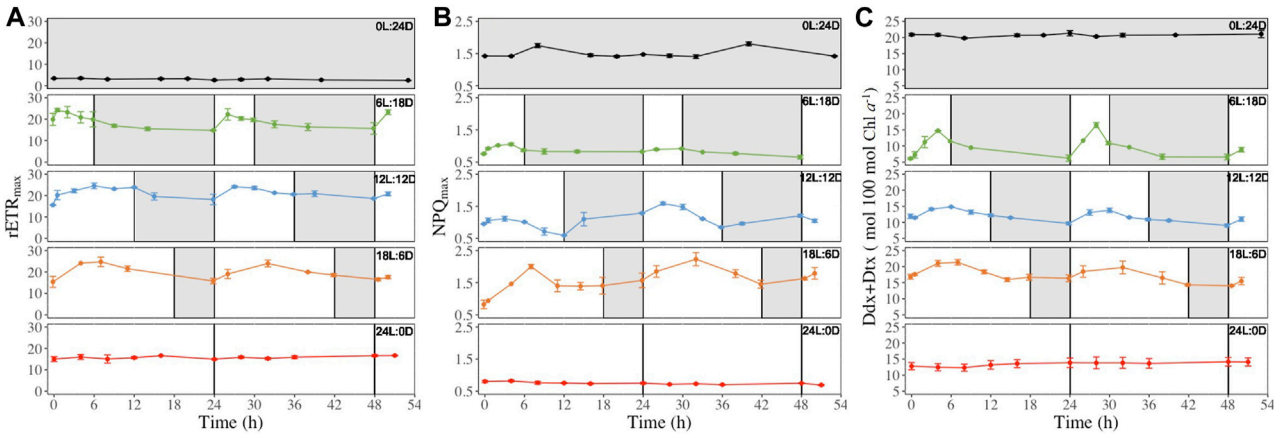

FIGURE 5
Maximum relative electron transport rate ($rETR_{max}$, μmol electrons m^{-2} s^{-1}, panel **(A)**, maximal non-photochemical quenching (NPQ_{max}, rel. unit, panel **(B)** and photoprotective xanthophyll pool per 100 mol chlorophylla (Ddx + Dtx, mol 100 mol Chl*a*$^{-1}$, panel **(C)** recorded at regular time points (see Figure 2) over 52 h in (F) *cylindrus* grown under five different photoperiods 0 h Light: 24 h Darkness (0L:24D), 6L:18D; 12L:12D; 18L:6D; 24L:0D. The white and grey sections correspond to light and darkness periods, respectively. Data are the mean values n = 3 ± SD. The same time series for the other parameters shown in Table 1 can be found in Supplementary Figures S2–S12. Data are the mean values n = 3 ± SD.

(Supplementary Figure S13) and the non-photochemical quenching parameters (Figures 6C, D). However, NPQmax (Figures 6C, G), ΦNPQ (Supplementary Figures S13B, E) which while having a maximum between the fourth to sixth hours of the ZT the maximum also coincides with 0.5 LD at the exception of Φ_{NPQ} 6L:18D where a maximum was reach during the dark period. Regarding pigments, only the β-carotene and Ddx + Dtx synthesis daily oscillations coincide with ZT (Figure 6D and supplementary 16. D), while fucoxanthin and the chlorophylls were not (Supplementary Figure S16).

4 Discussion

4.1 Photoacclimatation to increasing daylength

Fragilariopsis cylindrus grows efficiently under close to natural conditions, i.e., low temperature (0°C) and low light intensity (30 μmol photons m^{-2} s^{-1}), and it shows a maximum growth rate (0.25 ± 0.05 d^{-1}) in part with previous reports (Arrigo et al., 2010; Kropuenske et al., 2010; Morin et al., 2020; Croteau et al., 2021;

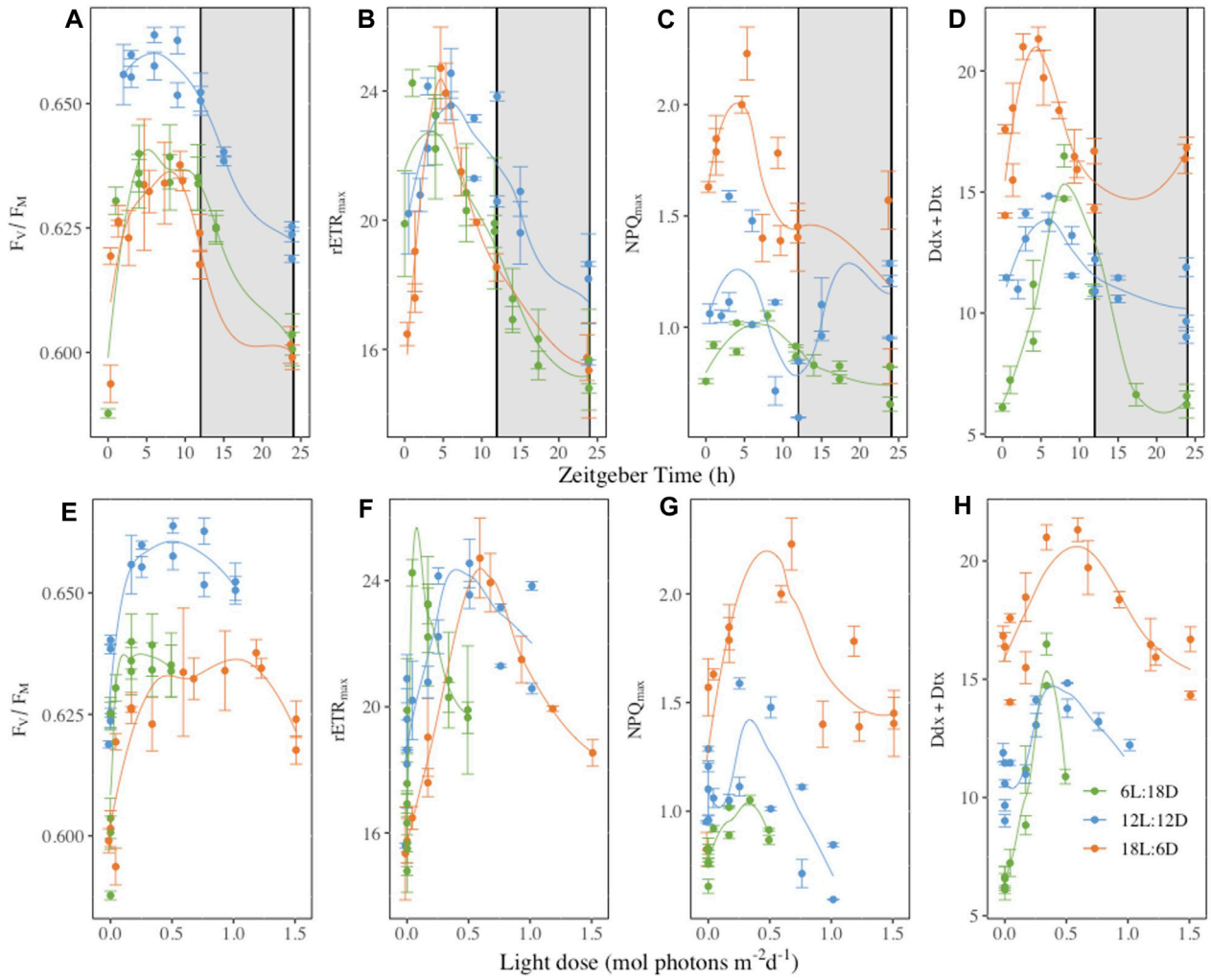

FIGURE 6
Dark-acclimated photochemical efficiency (F_V/F_M, rel. unit, panels **(A, D)**, maximum relative electron transport rate ($rETR_{max}$, µmol electrons m^{-2} s^{-1}, panels **(B, E)**, maximal non-photochemical quenching (NPQ_{max}, rel. unit, panels **(C, F)** and photoprotective xanthophyll pool per 100 mol chlorophyll *a* (Ddx + Dtx, mol 100 mol $Chla^{-1}$, panels **(D and G)** plotted as function of the Zeitgeber time (h, panels **(A–D)** or the light dose received during [mol photons m^{-2} d^{-1}, panels **(E–H)**]. Measurements were performed at regular time points over 52 h in *Fragilariopsis cylindrus* cells grown under three different photoperiods (6 h Light-L:18 h Darkness-D, 12L:12D; 18L:6D) (complete time series in Figures 2, 3, and Supplementary Figures S2–S12). Data are the mean values n = 3 ± SD, see Table 1 for parameters definition. Coloured lines are fitted curves (loess fit) of the mean value.

Croteau et al., 2022). High F_V/F_M and close C/N and Chl *a*/C values, as well as similar E_k and E_{opt} values, between photoperiods witnesses of healthy, non-nutrient limited and steady-state acclimated cultures (Frigstad et al., 2014; Niemi et al., 2015; Kvernvik et al., 2021). Using a light intensity which matches the growth optimum for *F. cylindrus* (Morin et al., 2020; Croteau et al., 2022), we observed a proportional growth rate increase with daylength until it reached a maximum with 18 h of light, i.e., further increase in daylength showed to have no further benefits (Guérin et al., 2022). This pattern is explained by a precise balance between the pigment content, photochemistry and photoprotection, which ultimately defines a certain level of production and growth at 0°C. *F. cylindrus* adjusted its light-harvesting and production capabilities with the light dose, i.e., with more light energy available it decreased its Fx content (but not Chl *c* and β-carotene), P-α as well as P_{max}, likely by adjusting the Rubisco content (Lacour et al., 2022), in order to maintain its investment in light energy harvesting *versus* C fixation (Chl *a*/C), as well as its optimal intensity for C fixation (P-E_k). In parallel, the maximal potential for NPQ (NPQ_{max}) increased proportionally with the total pool of xanthophylls Ddx + Dtx and Dtx content with constant DES (≈7%). This general pattern of response was achieved by precisely adjusting the PSII photochemical light energy usage *versus* energy losses as illustrated by similar values for effective (Φ_{PSII}, Φ_{NPQ}, Φ_{NO}) and maximal (F_V/F_M, $rETR_{max}$) parameters with 6 h, 12 h and 18 h daylength. This PSII activity adjustment was paralleled with the central maintenance of the light intensity range between the maximal *versus* the optimal photochemistry (E_{opt}/E_k).

This general picture however needs to be modulated with two main observations. First, the 6 h additional light from 6 L to 12 L and from 12 L to 18 L did not show the same features. With 12 h light, the light dose acclimation was close to reaching a plateau (reached with

18 h) while with 6 h, *F. cylindrus* did not reach its maximal acclimation capacity. This was illustrated by a lower Chl *a*/C and growth rate, when compared to 12L:12D conditions. Our second observation is the fact that when the photoperiod increases from 18 h to 24 h light, the response of cells was not directly related to the increase in light dose (from 2 to 2.67 mol photons m^{-2} d^{-1}), i.e., in addition the cells had to face the absence of regular darkness periods under 24 h day length. The combination of a higher light dose with the absence of regular darkness periods is known to respectively generate a stronger excitation pressure on PSII (Lepetit et al., 2013; Lepetit et al., 2017) and a disruption of photodamaged PSII repair in darkness (Xu et al., 2017), driving imbalance between functional and non-functional PSII, and a decrease in photosynthetic efficiency (Lavaud et al., 2016). Here, it was illustrated by a slightly but significantly lower F_V/F_M, Φ_{PSII} and $rETR_{max}$ which was nevertheless not reflected in P_{max} nor in the growth rate. The somewhat maintenance of photochemistry was ensured by a more effective dissipation of the excess light energy (Φ_{NPQ}) supported in part by a higher DES and content in Dtx. However, NPQ_{max} was stable, indicating that additional Dtx molecules were not all involved in NPQ (as illustrated by a lower NPQ_{max}/Dtx + Dtx), but instead likely participated in direct ROS scavenging (Lepetit et al., 2010; Lavaud and Lepetit, 2013; Schuurmans et al., 2015); and/or the number of Dtx binding sites, provided by LHCx proteins, was stable (Lepetit et al., 2013; Lepetit et al., 2017; Buck et al., 2019). It is noteworthy that the synthesis of additional Dtx molecules was *"de novo"*, i.e., with no change in Ddx content (Supplementary Figure S17), and it amounted to 1/3 of total Dtx by the end of the 24L:0D treatment monitoring. This feature was reported before in several temperate diatom species (Lavaud et al., 2004; Goss et al., 2006; Blommaert et al., 2017), and was hypothesised to bring additional photoprotection under strong and prolonged light stress (Lavaud and Lepetit, 2013; Blommaert et al., 2017). In parallel, the irradiance range where photochemistry is optimal/maximal was stretched (higher E_{opt}/E_k and $P\text{-}E_{opt}/P\text{-}E_k$) (Falkowski and Raven, 2013) and the induction of NPQ got closer to E_k ($E50_{NPQ}/E_k$ closer to 1), and the opposite to E_{opt}. This overall strategy allowed the cells to make the most of the excess in light energy without modifying their ability to harvest light (no major change in pigment content, in α and P-α), as proposed before (Lacour et al., 2020), driving a smooth transient acclimation towards 24L:0D conditions. However, mitigating constant illumination is more costly for the cells, as highlighted by the greater difference between NPP and GPP, compared to cells growing under light:dark cycle, which resulted in the observed lower growth rate.

Finally, it is worth noting the apparent discrepancy between photochemistry performances and production parameters: while the former are mainly similar among photoperiods (except for 24L:0D), the later showed a more contrasted response with a significantly higher P_{max} for the shortest daylength (6 h) and decreasing values with increasing daylength. Such pattern suggests that for 6L:18D, the rate of C fixation is likely maximized to compensate for the low light dose in order to provide the necessary energy to meet the needs for growth and nighttime processes (such as PSII repair; Xu et al., 2017). It therefore means that under 6L:18D most of the photosynthetic electrons are likely used for C fixation, while when daylength is longer (12 h–24 h) a larger proportion is diverted to other processes among which NPQ is not the major one as it does not tremendously increase, even under 24 h daylength. Such decoupling between the photochemical electron transport rate and C fixation is not uncommon in cold adapted diatoms (Goldman et al., 2015; Hancke et al., 2015; Lacour et al., 2017; Schuback et al., 2017; Lacour et al., 2022). These authors proposed that part of the photosynthetic electrons is used through alternative pathways to produce ATP and NAPDH before entering the Calvin cycle machinery, thus avoiding the need to reoxidize the newly fixed C, thus allowing a more efficient use of light energy. The evidence of such cyclic electron flow(s) has been specifically reported in *F. cylindrus* (Goldman et al., 2015; Lacour et al., 2017). This process may play a major role in the acclimation of *F. cylindrus*, and other polar diatoms, to changes in daylength and light dose, and it supports the above described fine tuning between light harvesting, photochemistry, photoprotection and production (Lacour et al., 2022).

4.2 Acclimation to continuous darkness

Acclimation of polar diatoms and *F. cylindrus* to prolonged darkness (from 7 days to 3 months) has been explored before (Mock et al., 2017; Kvernvik et al., 2018; Kennedy et al., 2019; Lacour et al., 2019; Morin et al., 2020; Joli et al., 2024). It showed a drastically different pattern than acclimation to photoperiods or continuous light. While PSII remained functional (high F_V/F_M), the maximal ($rETR_{max}$) and effective (Φ_{PSII}) photochemical efficiency, and the production (P_{max}), were dramatically lowered. We propose this is due to a decrease in the number of active, and possibly total, PSII (Lavaud et al., 2016), as also suggested by the decrease in β-carotene which is mainly associated with PSII reaction centers in diatoms (Nagao et al., 2020; Nagao et al., 2022). However, *F. cylindrus* was able to preserve its light-harvesting capacity as illustrated by the stable contents in photosynthetic pigments (Chl *a*, Chl *c* and Fx). Nevertheless, most of the harvested light energy was diverted to unregulated passive energy losses (high but similar Φ_{NO} compared to photoperiods) and NPQ (more than doubled Φ_{NPQ}), which explains the low remaining fraction used for photochemistry (2–3 times lower Φ_{PSII}). Because of the slowed photochemistry, and whole metabolism (Mock et al., 2017; Kennedy et al., 2019), a sudden return to light with an intact light-harvesting capacity will likely generate harmful photooxidative stress (Lacour et al., 2019; Morin et al., 2020). To prevent such situation, a high photoprotection potential needs to be ensured (Lacour et al., 2019; Morin et al., 2020). This was illustrated here by the largest pool size of Ddx + Dtx which, together with a high DES, ensured a strong constitutive content of Dtx, only overpassed by continuous light acclimation. As a result, NPQ_{max} was the highest (with the 18L:6D treatment) and it was directly related to the increased Φ_{NPQ} (contrary to 18L:6D). Additionally, to ensure an efficient induction of NPQ for weak but potentially stressful irradiances (Lacour et al., 2019; Morin et al., 2020), $E50_{NPQ}$ was lowered down (32.7 µmol photons m^{-2} s^{-1}) close to the intensity to which the cells were acclimated to, i.e. 30 µmol photons m^{-2} s^{-1}. Here too, but to a lower extent than under continuous light, NPQ_{max}/Dtx was <1 suggesting that probably many Dtx

molecules did not participate to NPQ but served as ROS scavengers (Lacour et al., 2020).

These results well support the crucial role that NPQ plays in allowing diatoms to maintain their light-harvesting capacity and the integrity of their PSII under changing light conditions, an ability that is especially crucial when metabolic rates are slowed down by low temperatures (Lacour et al., 2020). This is a straightforward way to make the best out of the rapidly changing light conditions at the bottom horizon and underneath the sea-ice during the end of winter through spring in the Arctic Ocean (Croteau et al., 2022) (see Figure 1). Especially, it helps polar diatoms to resume their photosynthetic productivity and growth rapidly and efficiently under extremely low light at the end of the polar night (Kvernvik et al., 2018; Randelhoff et al., 2020; Hoppe, 2021).

4.3 Photoperiodic regulation of photosynthesis

Most of the photosynthetic parameters (photochemistry and photoprotection) we measured showed repeated daily variations when cells were exposed to a light:darkness alternation with stable low light intensity. It holds true for the photoprotective pigments Ddx and Dtx, and to a lesser extent for β-carotene, but not for the chlorophylls nor Fx. Because of the relatively short duration of the monitoring (52 h) and the low sampling frequency (every 4 h maximum), a reliable cycle analysis of rhythmic oscillations was not possible. Nevertheless, data visualisation (as in Figures 4, 5) shows that photosynthetic parameters values and Ddx, Dtx contents mostly vary, with a rhythm modelled onto the light: darkness alternation over a ca. 24 h period, and that for most of them the period of rhythm depends on the daylength reaching their maximum before/around ZT 6 h, i.e., corresponding to the middle of the "day." However, due to the shorter daylength, several parameters did not follow this trend for the 6L:18D treatment, especially photoprotection parameters (Φ_{NPQ}, NPQ_{max}, Ddx, Dtx) were often controlled by the light dose in these conditions.

The photoperiodic rhythms shown by Φ_{PSII}, F_v/F_M and $rETR_{max}$ indicate a fine modulation of photochemistry in *F. cylindrus*. Interestingly, NPQ_{max} oscillated in parallel with these parameters, suggesting a strong link between the daily regulation of photochemistry and photoprotection capacity. Moreover, many of the photoprotection parameters (NPQ_{max}, Φ_{NPQ}, DES, Ddx and Dtx contents, Figure 6, Supplementary Figures S13, S15) showed a maximum around the middle of the light period, with the noticeable exception of DES under 18L:6D, which maximum was always reached earlier (during the first quarter of the light period). These observations demonstrate that NPQ is not a binary "ON/OFF" mechanism. Instead, it is finely regulated through a specific rhythm that is modelled onto the photoperiod, i.e., both the light:darkness alternation and the light dose. However, when the daylength is shorter, it appears that the modulation of NPQ extent is shifted toward a more direct light dose-dependent regulation.

The circadian rhythmicity of photosynthesis in higher plants, when measured via dynamic chlorophyll fluorescence, reflects an underlying inner ("endogenous") circadian clock regulation (Haydon et al., 2013; Dodd et al., 2015; Yarkhunova et al., 2018). In unicellular algae, a molecular circadian clock has been described only for a handful of species (Hu et al., 2017), including very few works dealing with rhythmic photosynthetic activity (Harding et al., 1981; Mackenzie and Morse, 2011). In the temperate model diatom *Phaeodactylum tricornutum*, there have been recent proofs for the existence of such circadian clock (Annunziata et al., 2019). With the present dataset, it is not possible to conclude on the existence of a circadian clock in *F. cylindrus*. Nevertheless, the question is open about the existence of an underlaying photoperiodic 24 h-based rhythmic regulation of the photosynthetic activity of *F. cylindrus*. Thanks to the recent sequencing of *F. cylindrus* genome (Mock et al., 2017), the analysis of *F. cylindrus* photoperiodic transcriptome will be essential to establish with certainty the nature of the observed rhythms, and the homology of the mechanisms in place in temperate and polar diatoms. Nonetheless, as shown here, non-destructive *in vivo* chlorophyll fluorescence appears to be an ideal tool for the integrative and comprehensive monitoring of photophysiology rhythms.

5 Conclusion

Our findings shed new light on the temporal rhythms that govern the photosynthetic machinery of the polar diatom *F. cylindrus* where it exists a photoperiodic 24 h-based rhythmic oscillation of certain aspects of the photophysiology, especially the PSII photochemistry and the NPQ-related photoprotection, including the synthesis of Ddx and Dtx xanthophylls. Because our experiments were performed in a controlled environment under constant low light at 0°C, the rhythmicity is not based on daily irradiance and temperature variations as reported during field campaigns (see for instance Schuback and Tortell, 2019). We believe that such photoperiodic rhythmicity likely supports the optimisation of the light harvesting and the use of light energy for C fixation via the daily fine-tuning of photochemistry and excess energy dissipation (NPQ), necessary under the extremely changing seasonal light conditions in the Arctic Ocean (see Figure 1). From our results, and previous ones (Lacour et al., 2020; Croteau et al., 2021; Guérin et al., 2022), it appears that the fine balance between photochemistry and photoprotection is essential, together with a strong capacity for NPQ, in supporting sustained production and growth despite low light and temperatures, over the broad range of photoperiods characteristic of the Arctic spring and fall light climates. Under the two extreme photoperiods of polar summer and winter, even if the rhythmicity of photosynthesis is lost, the ability for a strong NPQ is crucial for maintaining functional PSII and light-harvesting system, to be able to best exploit both extremely harsh and limiting irradiances at 0°C (Lacour et al., 2020). While the existence of an inner circadian clock in *F. cylindrus* remains uncertain, this research underscores the need for further exploration of the molecular processes governing photoperiodic regulation in polar diatoms.

These microorganisms play a vital role in polar ecosystems and offer insights into how life adapts to the challenges of climate change in these extreme environments. In an era of shifting polar environments due to climate change, understanding these intricate rhythms is a key to deciphering the resilience and adaptability of polar microalgae in a changing Arctic Ocean landscape. Indeed, with earlier snow and ice melt and shifting light conditions, the ability of *F. cylindrus*, and likely other polar diatoms, to grow under a wide range of photoperiods, and as soon as

the light intensity is sufficient (Randelhoff et al., 2020) may influence the timing and duration of algal blooms, subsequently shaping the availability of essential resources for higher trophic levels (Amiraux et al., 2022). However, while in the future algal blooms will likely occur earlier under shorter day length, algae will grow slower, as shown here. At higher light intensity, sympagic diatoms, like *F. cylindrus*, do not seem able to take advantage of the increase in the energy available at low temperatures and will likely not grow faster (Croteau et al., 2021; Guérin et al., 2022). Therefore, the duration of sea-ice blooms might be limited by the duration of the iced season and the melting rate of sea-ice. However, the warming surface waters (i.e., generating higher growth rate, Guérin et al., 2022) in conjunction with the increasing light intensity, might lead to a possible intensification and acceleration of phytoplankton diatom blooms, and increased primary production, depending on sufficient nutrient stocks (Ardyna and Arrigo, 2020).

In essence, our research not only delves into the intricacies of photophysiology, but also paints a portrait of resilience and adaptability in the face of Arctic environmental upheaval. Further research in this area is essential to grasp the broader consequences of climate change on polar diatom productivity and the ecosystem services it supports.

Data availability statement

The original contributions presented in the study are included in the article/Supplementary Material, further inquiries can be directed to the corresponding author.

Author contributions

SG: Conceptualization, Data curation, Formal Analysis, Investigation, Methodology, Validation, Visualization, Writing–original draft. FB: Data curation, Investigation, Methodology, Validation, Writing–review and editing. MG: Formal Analysis, Methodology, Resources, Writing–review and editing, Writing–original draft. MB: Formal Analysis, Funding acquisition, Resources, Supervision, Writing–review and editing. JL: Conceptualization, Data curation, Formal Analysis, Funding acquisition, Investigation, Methodology, Project administration, Resources, Supervision, Validation, Writing–original draft, Writing–review and editing.

Funding

The author(s) declare that financial support was received for the research, authorship, and/or publication of this article. This work was supported by the CNRS-Centre National de la Recherche Scientifique in the framework of the IRL Takuvik, the Canada Excellence Research Chair on Remote sensing of Canada's new Arctic Frontier (MB), the Sentinel North program of Université Laval supported in part by Canada First Research Excellence Fund (JL, projects 2.3 and SN-UiT), NSERC Canada Discovery (JL, RGPIN-2017-04505), the research network Québec-Océan, and Mitacs/Campus France.

Acknowledgments

The authors thank Mélanie Simard and Virginie Galindo for HPLC analyses, Thibaud Dezutter for CHN analyses, Joannie Ferland and Sarah-Michèle Cormier for technical help, Philippe Massicotte for statistical analyses support.

Conflict of interest

The authors declare that the research was conducted in the absence of any commercial or financial relationships that could be construed as a potential conflict of interest.

Publisher's note

Supplementary material

The Supplementary Material for this article can be found online at: https://www.frontiersin.org/articles/10.3389/fphbi.2024.1387119/full#supplementary-material

References

Amiraux, R., Lavaud, J., Cameron-Bergeron, K., Matthes, L. C., Peeken, I., Mundy, C. J., et al. (2022). Content in fatty acids and carotenoids in phytoplankton blooms during the seasonal sea ice retreat in Hudson Bay complex, Canada. *Elem. Sci. Anthropocene* 10, 00106. doi:10.1525/elementa.2021.00106

Andersen, R. A. (2005). *Algal Culturing Techniques*. Amsterdam: Burlington Elsevier/Academic Press.

Annunziata, R., Ritter, A., Fortunato, A. E., Manzotti, A., Cheminant-Navarro, S., Agier, N., et al. (2019). bHLH-PAS protein RITMO1 regulates diel biological rhythms in the marine diatom *Phaeodactylum tricornutum*. *Proc. Natl. Acad. Sci. U. S. A.* 116, 13137–13142. doi:10.1073/pnas.1819660116

Ardyna, M., and Arrigo, K. R. (2020). Phytoplankton dynamics in a changing Arctic Ocean. *Nat. Clim. Change* 10, 892–903. doi:10.1038/s41558-020-0905-y

Arrigo, K. R., Mills, M. M., Kropuenske, L. R., Van Dijken, G. L., Alderkamp, A. C., and Robinson, D. H. (2010). Photophysiology in two major southern ocean phytoplankton taxa: photosynthesis and growth of *Phaeocystis antarctica* and *Fragilariopsis cylindrus* under different irradiance levels. *Integr. Comp. Biol.* 50, 950–966. doi:10.1093/icb/icq021

Barnett, A., Meleder, V., Blommaert, L., Lepetit, B., Gaudin, P., Vyverman, W., et al. (2015). Growth form defines physiological photoprotective capacity in intertidal benthic diatoms. *ISME J.* 9, 32–45. doi:10.1038/ismej.2014.105

Blommaert, L., Huysman, M. J. J., Vyverman, W., Lavaud, J., and Sabbe, K. (2017). Contrasting NPQ dynamics and xanthophyll cycling in a motile and a non-motile intertidal benthic diatom. *Limnol. Oceanogr.* 62, 1466–1479. doi:10.1002/lno.10511

Büchel, C., Goss, R., Bailleul, B., Campbell, D., Lavaud, J., and Lepetit, B. (2022). "Photosynthetic light reactions in diatoms. I. The lipids and light-harvesting complexes

of the thylakoid membrane," in *The molecular life of diatoms*. Editors A. Falciatore and T. Mock (Switzerland: Springer International Publishing).

Buck, J. M., Sherman, J., Bartulos, C. R., Serif, M., Halder, M., Henkel, J., et al. (2019). Lhcx proteins provide photoprotection via thermal dissipation of absorbed light in the diatom *Phaeodactylum tricornutum*. *Nat. Commun.* 10, 4167. doi:10.1038/s41467-019-12043-6

Campbell, D. A., and Serôdio, J. (2020). "Photoinhibition of photosystem II in phytoplankton: processes and patterns," in *Photosynthesis in algae: biochemical and physiological mechanisms*. Berlin: Springer.

Croteau, D., Guérin, S., Bruyant, F., Ferland, J., Campbell, D. A., Babin, M., et al. (2021). Contrasting nonphotochemical quenching patterns under high light and darkness aligns with light niche occupancy in Arctic diatoms. *Limnol. Oceanogr.* 66, S231–S245. doi:10.1002/lno.11587

Croteau, D., Lacour, T., Schiffrine, N., Morin, P.-I., Forget, M.-H., Bruyant, F., et al. (2022). Shifts in growth light optima among diatom species support their succession during the spring bloom in the Arctic. *J. Ecol.* 110, 1356–1375. doi:10.1111/1365-2745.13874

Dodd, A. N., Belbin, F. E., Frank, A., and Webb, A. A. (2015). Interactions between circadian clocks and photosynthesis for the temporal and spatial coordination of metabolism. *Front. Plant Sci.* 6, 245. doi:10.3389/fpls.2015.00245

Eilers, P. H. C., and Peeters, J. C. H. (1988). A model for the relationship between light intensity and the rate of photosynthesis in phytoplankton. *Ecol. Model.* 42, 199–215. doi:10.1016/0304-3800(88)90057-9

Falciatore, A., Bailleul, B., Boulouis, A., Bouly, J.-P., Bujaldon, S., Cheminant-Navarro, S., et al. (2022). Light-driven processes: key players of the functional biodiversity in microalgae. *Comptes Rendus. Biol.* 345, 15–38. doi:10.5802/crbiol.80

Falkowski, P. G., and Raven, J. A. (2013). *Aquatic Photosynthesis: Second Edition*. Princeton, NJ:Princeton University Press.

Frigstad, H., Andersen, T., Bellerby, R. G. J., Silyakova, A., and Hessen, D. O. (2014). Variation in the seston C:N ratio of the Arctic Ocean and pan-Arctic shelves. *J. Mar. Syst.* 129, 214–223. doi:10.1016/j.jmarsys.2013.06.004

Goldman, J. A., Kranz, S. A., Young, J. N., Tortell, P. D., Stanley, R. H., Bender, M. L., et al. (2015). Gross and net production during the spring bloom along the Western Antarctic Peninsula. *New Phytol.* 205, 182–191. doi:10.1111/nph.13125

Goss, R., Ann Pinto, E., Wilhelm, C., and Richter, M. (2006). The importance of a highly active and DeltapH-regulated diatoxanthin epoxidase for the regulation of the PS II antenna function in diadinoxanthin cycle containing algae. *J. Plant Physiol.* 163, 1008–1021. doi:10.1016/j.jplph.2005.09.008

Goss, R., and Lepetit, B. (2015). Biodiversity of NPQ. *J. Plant Physiol.* 172, 13–32. doi:10.1016/j.jplph.2014.03.004

Guérin, S., Raguenes, L., Croteau, D., Babin, M., and Lavaud, J. (2022). Potential for the production of carotenoids of interest in the polar diatom *Fragilariopsis cylindrus*. *Mar. Drugs* 20, 491. doi:10.3390/md20080491

Guillard, R. R. L. (1975). "Culture of phytoplankton for feeding marine invertebrates," in *Culture of marine invertebrate animals: proceedings — 1st conference on culture of marine invertebrate animals greenport*. Editors W. L. Smith and M. H. Chanley (Boston, MA: Springer US).

Hancke, K., Dalsgaard, T., Sejr, M. K., Markager, S., and Glud, R. N. (2015). Phytoplankton productivity in an Arctic fjord (West Greenland): estimating electron requirements for carbon fixation and oxygen production. *PLoS One* 10, e0133275. doi:10.1371/journal.pone.0133275

Hancke, K., Lund-Hansen, L. C., Lamare, M. L., Højlund Pedersen, S., King, M. D., Andersen, P., et al. (2018). Extreme low light requirement for algae growth underneath sea ice: a case study from station Nord, NE Greenland. *J. Geophys. Res. Oceans* 123, 985–1000. doi:10.1002/2017jc013263

Haydon, M. J., Mielczarek, O., Robertson, F. C., Hubbard, K. E., and Webb, A. A. (2013). Photosynthetic entrainment of the *Arabidopsis thaliana* circadian clock. *Nature* 502, 689–692. doi:10.1038/nature12603

Hendrickson, L., Furbank, R. T., and Chow, W. S. (2004). A simple alternative approach to assessing the fate of absorbed light energy using chlorophyll fluorescence. *Photosynth Res.* 82, 73–81. doi:10.1023/B:PRES.0000040446.87305.f4

Hopes, A., Thomas, D. N., and Mock, T. (2017). "Polar microalgae: functional genomics, physiology, and the environment," in *Psychrophiles: from biodiversity to biotechnology*. Berlin: Springer.

Hoppe, C. J. M. (2021). "Always ready? primary production of Arctic phytoplankton at the end of the polar night," in *Limnology and oceanography letters*. Hoboken, NJ: Wiley.

Hu, Y., Vandenbussche, F., and Van der Straeten, D. (2017). Regulation of seedling growth by ethylene and the ethylene-auxin crosstalk. *Planta* 245, 467–489. doi:10.1007/s00425-017-2651-6

Joli, N., Concia, L., Mocaer, K., Guterman, J., Laude, J., Guerin, S., et al. (2024). Hypometabolism to survive the long polar night and subsequent successful return to light in the diatom Fragilariopsis cylindrus. *New Phytol.* 241, 2193–2208. doi:10.1111/nph.19387

Kennedy, F., Martin, A., Bowman, J. P., Wilson, R., and Mcminn, A. (2019). Dark metabolism: a molecular insight into how the Antarctic sea-ice diatom *Fragilariopsis cylindrus* survives long-term darkness. *New Phytol.* 223, 675–691. doi:10.1111/nph.15843

Klughammer, C., and Schreiber, U. (2008). "Complementary PS II quantum yields calculated from simple fluorescence parameters measured by PAM fluorometry and the saturation pulse method," in *PAM application notes*. Effeltrich: Heinz Walz GmbH, 27–35.

Kropuenske, L. R., Mills, M. M., Van Dijken, G. L., Alderkamp, A.-C., Mine Berg, G., Robinson, D. H., et al. (2010). Strategies and rates of photoacclimation in two major southern ocean phytoplankton taxa: p*haeocystis Antarctica* (Haptophyta) and *Fragilariopsis Cylindrus* (Bacillariophyceae)1. *J. Phycol.* 46, 1138–1151. doi:10.1111/j.1529-8817.2010.00922.x

Kropuenske, L. R., Mills, M. M., Van Dijken, G. L., Bailey, S., Robinson, D. H., Welschmeyer, N. A., et al. (2009). Photophysiology in two major Southern Ocean phytoplankton taxa: photoprotection in *Phaeocystis antarctica* and *Fragilariopsis cylindrus*. *Limnol. Oceanogr.* 54, 1176–1196. doi:10.4319/lo.2009.54.4.1176

Kvernvik, A. C., Hoppe, C. J. M., Greenacre, M., Verbiest, S., Wiktor, J. M., Gabrielsen, T. M., et al. (2021). Arctic sea ice algae differ markedly from phytoplankton in their ecophysiological characteristics. *Mar. Ecol. Prog. Ser.* 666, 31–55. doi:10.3354/meps13675

Kvernvik, A. C., Hoppe, C. J. M., Lawrenz, E., Prasil, O., Greenacre, M., Wiktor, J. M., et al. (2018). Fast reactivation of photosynthesis in arctic phytoplankton during the polar night. *J. Phycol.* 54, 461–470. doi:10.1111/jpy.12750

Lacour, T., Babin, M., and Lavaud, J. (2020). Diversity in xanthophyll cycle pigments content and related nonphotochemical quenching (NPQ) among microalgae: implications for growth strategy and ecology. *J. Phycol.* 56, 245–263. doi:10.1111/jpy.12944

Lacour, T., Larivière, J., and Babin, M. (2017). Growth, *Chl a* content, photosynthesis, and elemental composition in polar and temperate microalgae. *Limnol. Oceanogr.* 62, 43–58. doi:10.1002/lno.10369

Lacour, T., Larivière, J., Ferland, J., Bruyant, F., Lavaud, J., and Babin, M. (2018). The role of sustained photoprotective non-photochemical quenching in low temperature and high light acclimation in the bloom-forming arctic diatom *Thalassiosira gravida*.*Front. Mar. Sci.* 5, 354. doi:10.3389/fmars.2018.00354

Lacour, T., Lariviere, J., Ferland, J., Morin, P. I., Grondin, P. L., Donaher, N., et al. (2022). Photoacclimation of the polar diatom *Chaetoceros neogracilis* at low temperature. *PLoS One* 17, e0272822. doi:10.1371/journal.pone.0272822

Lacour, T., Morin, P.-I., Sciandra, T., Donaher, N., Campbell, D. A., Ferland, J., et al. (2019). Decoupling light harvesting, electron transport and carbon fixation during prolonged darkness supports rapid recovery upon re-illumination in the Arctic diatom *Chaetoceros neogracilis*. *Polar Biol.* 42, 1787–1799. doi:10.1007/s00300-019-02507-2

Lavaud, J., and Goss, R. (2014). "The peculiar features of non-photochemical fluorescence quenching in diatoms and brown algae," in *Non-photochemical quenching and energy dissipation in plants, algae and cyanobacteria*. Berlin: Springer.

Lavaud, J., and Lepetit, B. (2013). An explanation for the inter-species variability of the photoprotective non-photochemical chlorophyll fluorescence quenching in diatoms. *Biochim. Biophys. Acta* 1827, 294–302. doi:10.1016/j.bbabio.2012.11.012

Lavaud, J., Rousseau, B., and Etienne, A. L. (2004). General features of photoprotection by energy dissipation in planktonic diatoms (Bacillariophyceae)1. *J. Phycol.* 40, 130–137. doi:10.1046/j.1529-8817.2004.03026.x

Lavaud, J., Six, C., and Campbell, D. A. (2016). Photosystem II repair in marine diatoms with contrasting photophysiologies. *Photosynth Res.* 127, 189–199. doi:10.1007/s11120-015-0172-3

Lavoie, M., Saint-Beat, B., Strauss, J., Guérin, S., Allard, A. S. V. H., Falciatore, A., et al. (2020). Genome-scale metabolic reconstruction and *in silico* perturbation analysis of the polar diatom *Fragilariopsis cylindrus* predicts high metabolic robustness. *Biology* 9, 30. doi:10.3390/biology9020030

Lepetit, B., Campbell, D., Lavaud, J., Büchel, C., Goss, R., and Bailleul, B. (2022). "Photosynthetic light reactions in diatoms. II. The dynamic regulation of the various light reactions," in *The molecular life of diatoms*. Editors A. Falciatore and T. Mock (Switzerland: Springer International Publishing).

Lepetit, B., Gelin, G., Lepetit, M., Sturm, S., Vugrinec, S., Rogato, A., et al. (2017). The diatom *Phaeodactylum tricornutum* adjusts nonphotochemical fluorescence quenching capacity in response to dynamic light via fine-tuned Lhcx and xanthophyll cycle pigment synthesis. *New Phytol.* 214, 205–218. doi:10.1111/nph.14337

Lepetit, B., Sturm, S., Rogato, A., Gruber, A., Sachse, M., Falciatore, A., et al. (2013). High light acclimation in the secondary plastids containing diatom Phaeodactylum tricornutum is triggered by the redox state of the plastoquinone pool. *Plant Physiol.* 161, 853–865. doi:10.1104/pp.112.207811

Lepetit, B., Volke, D., Gilbert, M., Wilhelm, C., and Goss, R. (2010). Evidence for the existence of one antenna-associated, lipid-dissolved and two protein-bound pools of diadinoxanthin cycle pigments in diatoms. *Plant Physiol.* 154, 1905–1920. doi:10.1104/pp.110.166454

Leu, E., Mundy, C. J., Assmy, P., Campbell, K., Gabrielsen, T. M., Gosselin, M., et al. (2015). Arctic spring awakening – steering principles behind the phenology of vernal ice algal blooms. *Prog. Oceanogr.* 139, 151–170. doi:10.1016/j.pocean.2015.07.012

Li, G., Woroch, A. D., Donaher, N. A., Cockshutt, A. M., and Campbell, D. A. (2016). A hard day's night: diatoms continue recycling photosystem II in the dark. *Front. Mar. Sci.* 3, 218. doi:10.3389/fmars.2016.00218

Macintyre, H. L., Kana, T. M., and Geider, R. J. (2000). The effect of water motion on short-term rates of photosynthesis by marine phytoplankton. *Trends Plant Sci.* 5, 12–17. doi:10.1016/s1360-1385(99)01504-6

Massicotte, P., Amiraux, R., Amyot, M.-P., Archambault, P., Ardyna, M., Arnaud, L., et al. (2020). Green Edge ice camp campaigns: understanding the processes controlling the under-ice Arctic phytoplankton spring bloom. *Earth Syst. Sci. Data* 12, 151–176. doi:10.5194/essd-12-151-2020

Mayot, N., Matrai, P., Ellingsen, I. H., Steele, M., Johnson, K., Riser, S. C., et al. (2018). Assessing phytoplankton activities in the seasonal ice zone of the Greenland sea over an annual cycle. *J. Geophys. Res. Oceans* 123, 8004–8025. doi:10.1029/2018jc014271

Mock, T., Otillar, R. P., Strauss, J., Mcmullan, M., Paajanen, P., Schmutz, J., et al. (2017). Evolutionary genomics of the cold-adapted diatom *Fragilariopsis cylindrus*. *Nature* 541, 536–540. doi:10.1038/nature20803

Morin, P. I., Lacour, T., Grondin, P. L., Bruyant, F., Ferland, J., Forget, M. H., et al. (2020). Response of the sea-ice diatom *Fragilariopsis cylindrus* to simulated polar night darkness and return to light. *Limnol. Oceanogr.* 65, 1041–1060. doi:10.1002/lno.11368

Nagao, R., Kato, K., Ifuku, K., Suzuki, T., Kumazawa, M., Uchiyama, I., et al. (2020). Structural basis for assembly and function of a diatom photosystem I-light-harvesting supercomplex. *Nat. Commun.* 11, 2481. doi:10.1038/s41467-020-16324-3

Nagao, R., Kato, K., Kumazawa, M., Ifuku, K., Yokono, M., Suzuki, T., et al. (2022). Structural basis for different types of hetero-tetrameric light-harvesting complexes in a diatom PSII-FCPII supercomplex. *Nat. Commun.* 13, 1764. doi:10.1038/s41467-022-29294-5

Nicolaus, M., Gerland, S., Hudson, S. R., Hanson, S., Haapala, J., and Perovich, D. K. (2010). Seasonality of spectral albedo and transmittance as observed in the Arctic Transpolar Drift in 2007. *J. Geophys Res. Atmos.* 115, C11011. doi:10.1029/2009jc006074

Niemi, A., Michel, C., Deming, J. W., and Thomsen, L. (2015). Temporal and spatial variability in sea-ice carbon:nitrogen ratios on Canadian Arctic shelves. *Elem. Sci. Anthropocene* 3, 000078. doi:10.12952/journal.elementa.000078

Ni, G., Zimbalatti, G., Murphy, C. D., Barnett, A. B., Arsenault, C. M., Li, G., et al. (2017). Arctic *Micromonas* uses protein pools and non-photochemical quenching to cope with temperature restrictions on Photosystem II protein turnover. *Photosynth Res.* 131, 203–220. doi:10.1007/s11120-016-0310-6

Oziel, L., Massicotte, P., Randelhoff, A., Ferland, J., Vladoiu, A., Lacour, L., et al. (2019). Environmental factors influencing the seasonal dynamics of spring algal blooms in and beneath sea ice in western Baffin Bay. *Elem. Sci. Anthropocene* 7, 34. doi:10.1525/elementa.372

Petrou, K., Hill, R., Brown, C. M., Campbell, D. A., Doblin, M. A., and Ralph, P. J. (2010). Rapid photoprotection in sea-ice diatoms from the East Antarctic pack ice. *Limnol. Oceanogr.* 55, 1400–1407. doi:10.4319/lo.2010.55.3.1400

Petrou, K., Kranz, S. A., Trimborn, S., Hassler, C. S., Ameijeiras, S. B., Sackett, O., et al. (2016). Southern Ocean phytoplankton physiology in a changing climate. *J. Plant Physiol.* 203, 135–150. doi:10.1016/j.jplph.2016.05.004

Randelhoff, A., Lacour, L., Marec, C., Leymarie, E., Lagunas, J., Xing, X., et al. (2020). Arctic mid-winter phytoplankton growth revealed by autonomous profilers. *Sci. Adv.* 6, eabc2678. doi:10.1126/sciadv.abc2678

Rantanen, M., Karpechko, A. Y., Lipponen, A., Nordling, K., Hyvärinen, O., Ruosteenoja, K., et al. (2022). The Arctic has warmed nearly four times faster than the globe since 1979. *Commun. Earth Environ.* 3, 168. doi:10.1038/s43247-022-00498-3

Schuback, N., Hoppe, C. J. M., Tremblay, J.-É., Maldonado, M. T., and Tortell, P. D. (2017). Primary productivity and the coupling of photosynthetic electron transport and carbon fixation in the Arctic Ocean. *Limnol. Oceanogr.* 62, 898–921. doi:10.1002/lno.10475

Schuback, N., and Tortell, P. D. (2019). Diurnal regulation of photosynthetic light absorption, electron transport and carbon fixation in two contrasting oceanic environments. *Biogeosciences* 16, 1381–1399. doi:10.5194/bg-16-1381-2019

Schuurmans, R. M., Van Alphen, P., Schuurmans, J. M., Matthijs, H. C., and Hellingwerf, K. J. (2015). Comparison of the photosynthetic yield of cyanobacteria and green algae: different methods give different answers. *PLoS One* 10, e0139061. doi:10.1371/journal.pone.0139061

Serodio, J., and Lavaud, J. (2011). A model for describing the light response of the nonphotochemical quenching of chlorophyll fluorescence. *Photosynth Res.* 108, 61–76. doi:10.1007/s11120-011-9654-0

Steeman-Nielsen, E. (1975). *Marine Photosynthesis*. New York, NY: Elsevier Science.

Taddei, L., Stella, G. R., Rogato, A., Bailleul, B., Fortunato, A. E., Annunziata, R., et al. (2016). Multisignal control of expression of the LHCX protein family in the marine diatom Phaeodactylum tricornutum. *J. Exp. Bot.* 67, 3939–3951. doi:10.1093/jxb/erw198

Wilhelm, C., Jungandreas, A., Jakob, T., and Goss, R. (2014). Light acclimation in diatoms: from phenomenology to mechanisms. *Mar. Genomics* 16, 5–15. doi:10.1016/j.margen.2013.12.003

Xu, K., Grant-Burt, J. L., Donaher, N., and Campbell, D. A. (2017). Connectivity among Photosystem II centers in phytoplankters: patterns and responses. *Biochim. Biophys. Acta Bioenerg.* 1858, 459–474. doi:10.1016/j.bbabio.2017.03.003

Xu, K., Lavaud, J., Perkins, R., Austen, E., Bonnanfant, M., and Campbell, D. A. (2019). Phytoplankton σPSII and excitation dissipation; implications for estimates of primary productivity. *Front. Mar. Sci.* 5, 281. doi:10.3389/fmars.2018.00281

Yarkhunova, Y., Guadagno, C. R., Rubin, M. J., Davis, S. J., Ewers, B. E., and Weinig, C. (2018). Circadian rhythms are associated with variation in photosystem II function and photoprotective mechanisms. *Plant Cell Environ.* 41, 2518–2529. doi:10.1111/pce.13216

Young, J. N., and Schmidt, K. (2020). It's what's inside that matters: physiological adaptations of high-latitude marine microalgae to environmental change. *New Phytol.* 227, 1307–1318. doi:10.1111/nph.16648

Zapata, M., Rodríguez, F. C., and Garrido, J. L. (2000). Separation of chlorophylls and carotenoids from marine phytoplankton: a new HPLC method using a reversed phase C8 column and pyridine-containing mobile phases. *Mar. Ecol. Prog. Ser.* 195, 29–45. doi:10.3354/meps195029